SUPPLEMENT TO:

THE LOCOMOTOR ECOMORPHOLOGY OF MESOZOIC MARINE REPTILES

by SUSANA GUTARRA*[,1,2], THOMAS L. STUBBS[1], BENJAMIN C. MOON[1], BEATRICE H. HEIGHTON and MICHAEL J. BENTON[1]

[1]School of Earth Sciences, University of Bristol, Life Sciences Building, 24 Tyndall Avenue, Bristol BS8 1TQ, UK; *email: susana.gutarradiaz@bristol.ac.uk

[2]Department of Earth Sciences, the Natural History Museum, Cromwell Road, London, SW7 5BD, UK

Contents:

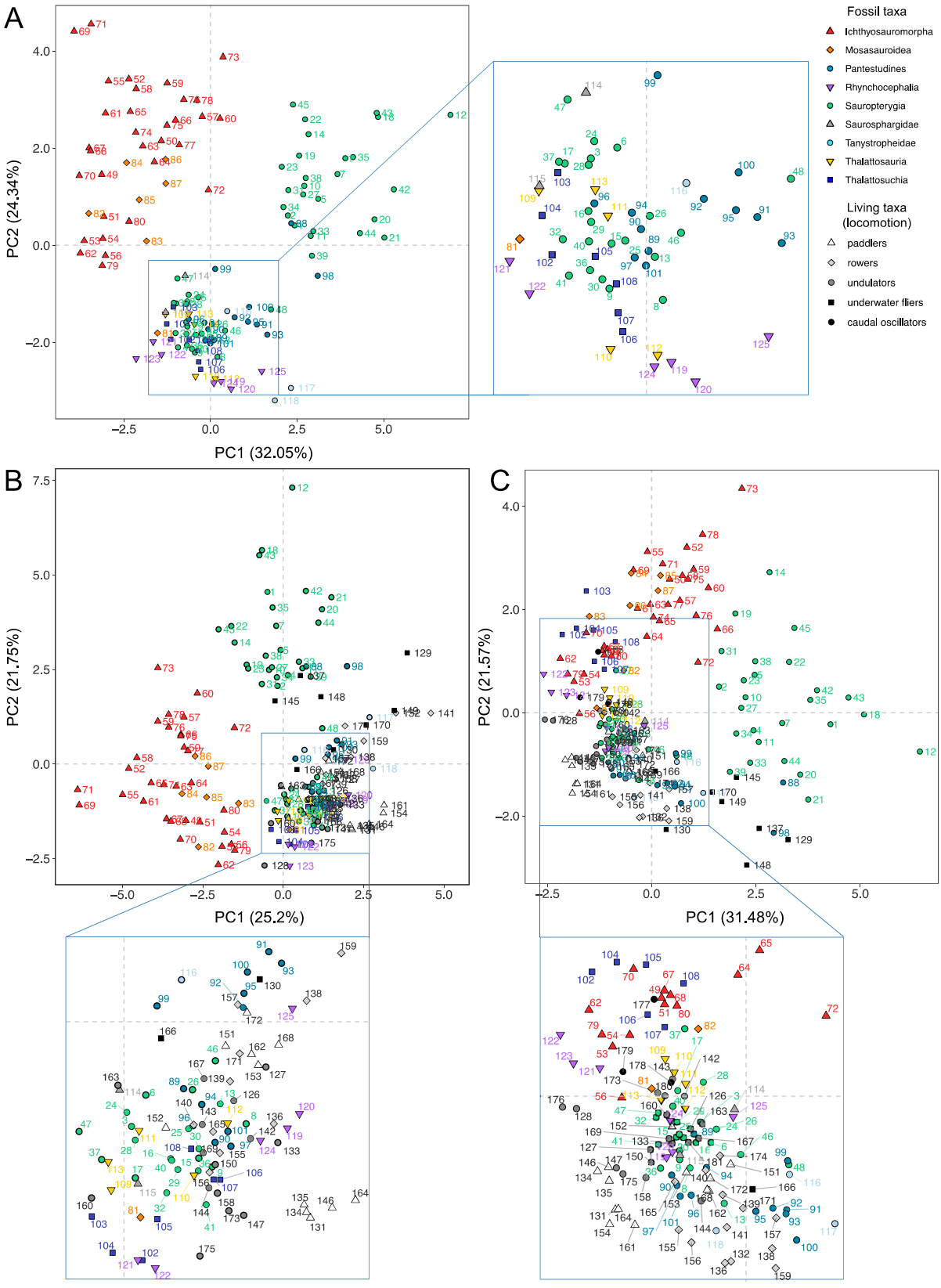

Fig.S1 Labelled morphospace plots for Mesozoic marine reptiles and extant tetrapods. (A) Bivariate plot of PC1–2 for Mesozoic marine reptiles, as in Fig. 2A, showing taxa distribution with numbered labels. (B, C) Plots of PC 1–2 for the morphospace of living and extinct taxa using all functional characters (B) or a reduced version excluding the hindlimb characters (C), as in Fig. 2C and D respectively. Areas of high density of taxa are enclosed in a blue frame and amplified next to each plot.

D

	Taxon	Clade		Taxon	Clade		Taxon	Clade
1	*Albertonectes vanderveldei*	Sauropt.	62	*Hupehsuchus nanchangensis*	Ichthyo.	123	*Pleurosaurus goldfussi*	Rhyncho.
2	*Archaeonectrus rostratus*	Sauropt.	63	*Ichthyosaurus communis*	Ichthyo.	124	*Sapheosaurus thiollierei*	Rhyncho.
3	*Atopodentatus unicus*	Sauropt.	64	*Ichthyosaurus larkini*	Ichthyo.	125	*Vadasaurus herzogi*	Rhyncho.
4	*Attenborosaurus conybeari*	Sauropt.	65	*Ichthyosaurus somersetensis*	Ichthyo.	126	*Alligator mississipiens*	Liv. reptile
5	*Atychodracon megacephalus*	Sauropt.	66	*Leptonectes tenuirostris*	Ichthyo.	127	*Amblyrhynchus cristatus*	Liv. reptile
6	*Ceresiosaurus calcagnii*	Sauropt.	67	*Mixosaurus cornalianus*	Ichthyo.	128	*Andrias japonicus*	Liv. amphibian
7	*Cryptoclidus eurymerus*	Sauropt.	68	*Mixosaurus xindianensis*	Ichthyo.	129	*Aptenodytes patagonicus*	Liv. bird
8	*Diandongosaurus acutidentatus*	Sauropt.	69	*Ophthalmosaurus icenicus*	Ichthyo.	130	*Arctocephalus pusillus*	Liv. mammal
9	*Dianmeisaurus gracilis*	Sauropt.	70	*Phalarodon atavus*	Ichthyo.	131	*Arvicola terrestris*	Liv. mammal
10	*Dolichorhynchops osborni*	Sauropt.	71	*Platypterygius hercynicus*	Ichthyo.	132	*Bufo bufo*	Liv. amphibian
11	*Hauffiosaurus zanoni*	Sauropt.	72	*Qianichthyosaurus zhoui*	Ichthyo.	133	*Caiman latirostris*	Liv. reptile
12	*Hydrotherosaurus alexandrae*	Sauropt.	73	*Shonisaurus popularis*	Ichthyo.	134	*Castor canadiensis*	Liv. mammal
13	*Keichousaurus hui*	Sauropt.	74	*Stenopterygius quadriscissus*	Ichthyo.	135	*Castor fiber*	Liv. mammal
14	*Kronosaurus boyacensis*	Sauropt.	75	*Stenopterygius triscissus*	Ichthyo.	136	*Chelodina longicollis*	Liv. reptile
15	*Lariosaurus balsami*	Sauropt.	76	*Stenopterygius uniter*	Ichthyo.	137	*Chelonia mydas*	Liv. reptile
16	*Lariosaurus valceresii*	Sauropt.	77	*Suevoleviathan integer*	Ichthyo.	138	*Chelus fimbriata*	Liv. reptile
17	*Lariosaurus xingyiensis*	Sauropt.	78	*Temnodontosaurus trigonodon*	Ichthyo.	139	*Chelydra serpentina*	Liv. reptile
18	*Libonectes atlasense*	Sauropt.	79	*Utatsusaurus hataii*	Ichthyo.	140	*Chitra chitra*	Liv. reptile
19	*Liopleurodon ferox*	Sauropt.	80	*Xinminosaurus catactes*	Ichthyo.	141	*Cornufer guppyi*	Liv. amphibian
20	*Meyerasaurus victor*	Sauropt.	81	*Aigialosaurus bucchichi*	Mosasaur.	142	*Crocodylus intermedius*	Liv. reptile
21	*Microcleidus brachypterygius*	Sauropt.	82	*Halisaurus sternbergii*	Mosasaur.	143	*Crocodylus porosus*	Liv. reptile
22	*Morenosaurus stocki*	Sauropt.	83	*Clidastes prophyton*	Mosasaur.	144	*Cryptobranchus alleganiensis*	Liv. amphibian
23	*Muraenosaurus leedsii*	Sauropt.	84	*Mosasaurus lemonnieri*	Mosasaur.	145	*Dermochelys coriacea*	Liv. reptile
24	*Neusticosaurus edwardsii*	Sauropt.	85	*Plotosaurus bennisoni*	Mosasaur.	146	*Desmana moschata*	Liv. mammal
25	*Neusticosaurus peyeri*	Sauropt.	86	*Platecarpus tympaniticus*	Mosasaur.	147	*Enhydra lutris*	Liv. mammal
26	*Neusticosaurus pusillus*	Sauropt.	87	*Tylosaurus proriger*	Mosasaur.	148	*Eremtochelys imbricata*	Liv. reptile
27	*Nichollssaura borealis*	Sauropt.	88	*Archelon ischyros*	Pantestud.	149	*Eudyptes chrysocome*	Liv. bird
28	*Nothosaurus giganteus*	Sauropt.	89	*Eorhynchochelys sinensis*	Pantestud.	150	*Halichoerus grypus*	Liv. mammal
29	*Nothosaurus youngi*	Sauropt.	90	*Eurysternum wagleri*	Pantestud.	151	*Hexaprotodon liberiensis*	Liv. mammal
30	*Paraplacodus broilii*	Sauropt.	91	*Hoyasemys jimenezi*	Pantestud.	152	*Hippopotamus amphibus*	Liv. mammal
31	*Peloneustes philarchus*	Sauropt.	92	*Idiochelys fitzingeri*	Pantestud.	153	*Hydrochoerus hydrochaeris*	Liv. mammal
32	*Placodus inexpectatus*	Sauropt.	93	*Jeholochelys lingyuanensis*	Pantestud.	154	*Hydromys sp.*	Liv. mammal
33	*Plesiopterys wildi*	Sauropt.	94	*Odontochelys semitestacea*	Pantestud.	155	*Kinosternon acutum*	Liv. reptile
34	*Plesiosaurus* sp.	Sauropt.	95	*Ordosemys liaoxiensis*	Pantestud.	156	*Kinosternon subrubrum*	Liv. reptile
35	*Polycotylus latipinnis*	Sauropt.	96	*Platychelys oberndorferi*	Pantestud.	157	*Lissemys punctata*	Liv. reptile
36	*Psephochelys polyosteoderma*	Sauropt.	97	*Proganochelys quenstedti*	Pantestud.	158	*Lutra lutra*	Liv. mammal
37	*Psephoderma alpinum*	Sauropt.	98	*Protostega gigas*	Pantestud.	159	*Mesoclemmys nasuta*	Liv. reptile
38	*Rhomaleosaurus cramptoni*	Sauropt.	99	*Rhinochelys nammourensis*	Pantestud.	160	*Mirounga leonina*	Liv. mammal
39	*Seeleyosaurus guilelmiimperatoris*	Sauropt.	100	*Toxochelys latiremis*	Pantestud.	161	*Myocastor coypus*	Liv. mammal
40	*Serpianosaurus mirigiolensis*	Sauropt.	101	*Xinjiangchelys wusu*	Pantestud.	162	*Neovison vison*	Liv. mammal
41	*Sinocyamodus xinpuensis*	Sauropt.	102	*Cricosaurus bambergensis*	Thalattosu.	163	*Odobenus rosmarus*	Liv. mammal
42	*Stenorhynchosaurus munozi*	Sauropt.	103	*Cricosaurus suevicus*	Thalattosu.	164	*Ondatra zybethicus*	Liv. mammal
43	*Styxosaurus* sp.	Sauropt.	104	*Dakosaurus maximus*	Thalattosu.	165	*Ornithorhynchus anatinus*	Liv. mammal
44	*Thalassiodracon hawkinsii*	Sauropt.	105	*Metriorhynchus superciliosus*	Thalattosu.	166	*Otaria byronia*	Liv. mammal
45	*Thalassomedon haningtoni*	Sauropt.	106	*Pelagosaurus typus*	Thalattosu.	167	*Phoca vitulina*	Liv. mammal
46	*Wangosaurus brevirostris*	Sauropt.	107	*Platysuchus multicrobiculatus*	Thalattosu.	168	*Potamogale velox*	Liv. mammal
47	*Wumengosaurus delicatomandibularis*	Sauropt.	108	*Steneosaurus bollensis*	Thalattosu.	169	*Pteronura brasiliensis*	Liv. mammal
48	*Yunguisaurus liae*	Sauropt.	109	*Anshunsaurus huangguoshuensis*	Thalattosa.	170	*Spheniscus demersus*	Liv. bird
49	*Barracudasauroides panxianensis*	Ichthyo.	110	*Askeptosaurus italicus*	Thalattosa.	171	*Staurotypus triporcatus*	Liv. reptile
50	*Besanosaurus leptorhynchus*	Ichthyo.	111	*Clarazia schinzi*	Thalattosa.	172	*Tapirus indicus*	Liv. mammal
51	*Cartorhynchus lenticarpus*	Ichthyo.	112	*Endennasaurus acutirostris*	Thalattosa.	173	*Tomistoma schlegelii*	Liv. reptile
52	*Caypullysaurus bonapartei*	Ichthyo.	113	*Miodentosaurus brevis*	Thalattosa.	174	*Tryonyx triunguis*	Liv. reptile
53	*Chaohusaurus brevifemoralis*	Ichthyo.	114	*Helveticosurus zollingeri*	Saurosphar.	175	*Varanus niloticus*	Liv. reptile
54	*Chaohusaurus chaoxianensis*	Ichthyo.	115	*Largocephalosaurus qianensis*	Saurosphar.	176	*Amphiuma means*	Liv. amphibian
55	*Cryopterygius kristiansenae*	Ichthyo.	116	*Dinocephalosaurus orientalis*	Tanystroph.	177	*Delphinus delphis*	Liv. mammal
56	*Eretmorhipis carroldongi*	Ichthyo.	117	*Tanystropheus longobardicus*	Tanystroph.	178	*Dugong dugon*	Liv. mammal
57	*Eurhinosaurus longirostris*	Ichthyo.	118	*Tanytrachelos ahynis*	Tanystroph.	179	*Phocoena phocoena*	Liv. mammal
58	*Excalibosaurus costini*	Ichthyo.	119	*Kallimodon cerinensis*	Rhyncho.	180	*Trichechus manatus*	Liv. mammal
59	*Guanlingsaurus lingae*	Ichthyo.	120	*Kallimodon pulchellus*	Rhyncho.	181	*Trichechus senegalensis*	Liv. mammal
60	*Guizhouichthyosaurus tangae*	Ichthyo.	121	*Palaeopleurosaurus posidoniae*	Rhyncho.			
61	*Hauffiopteryx typicus*	Ichthyo.	122	*Pleurosaurus ginsburgi*	Rhyncho.			

Fig. S1 (Continued from previous page) (D) List of numbers and corresponding taxa.

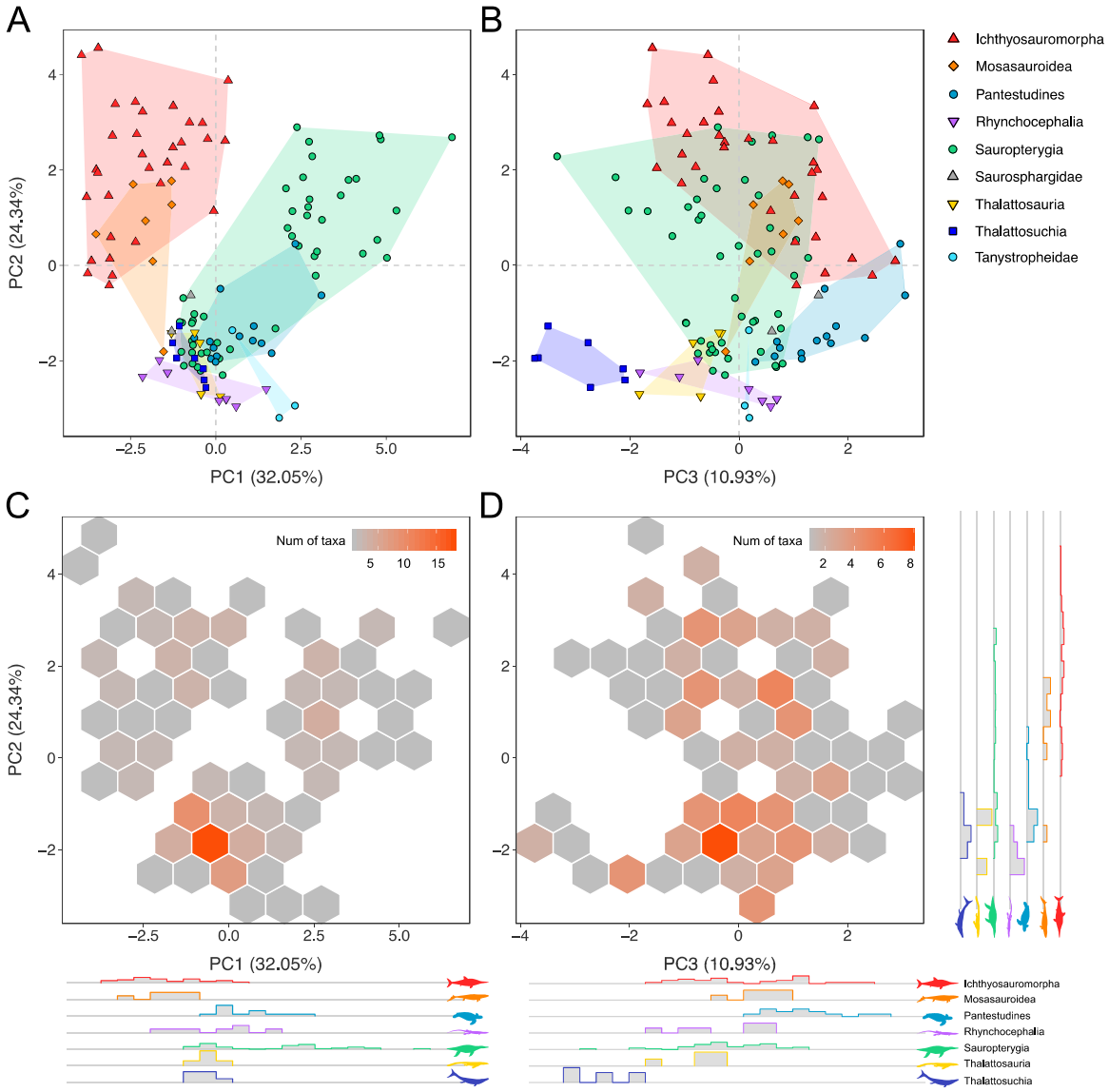

Fig. S2. Morphospace occupation and density distribution. (A, B) Bidimensional plots of the three main axis of variation PC1–2 (A) and PC2–3 (B) showing the distribution of the main groups of Mesozoic marine reptiles. (C, D) Hexbin plot showing the concentration of taxa across the morphospace area. Individual histograms showing the distribution of the main groups along each axis are shown at the bottom and right sides of the main plot.

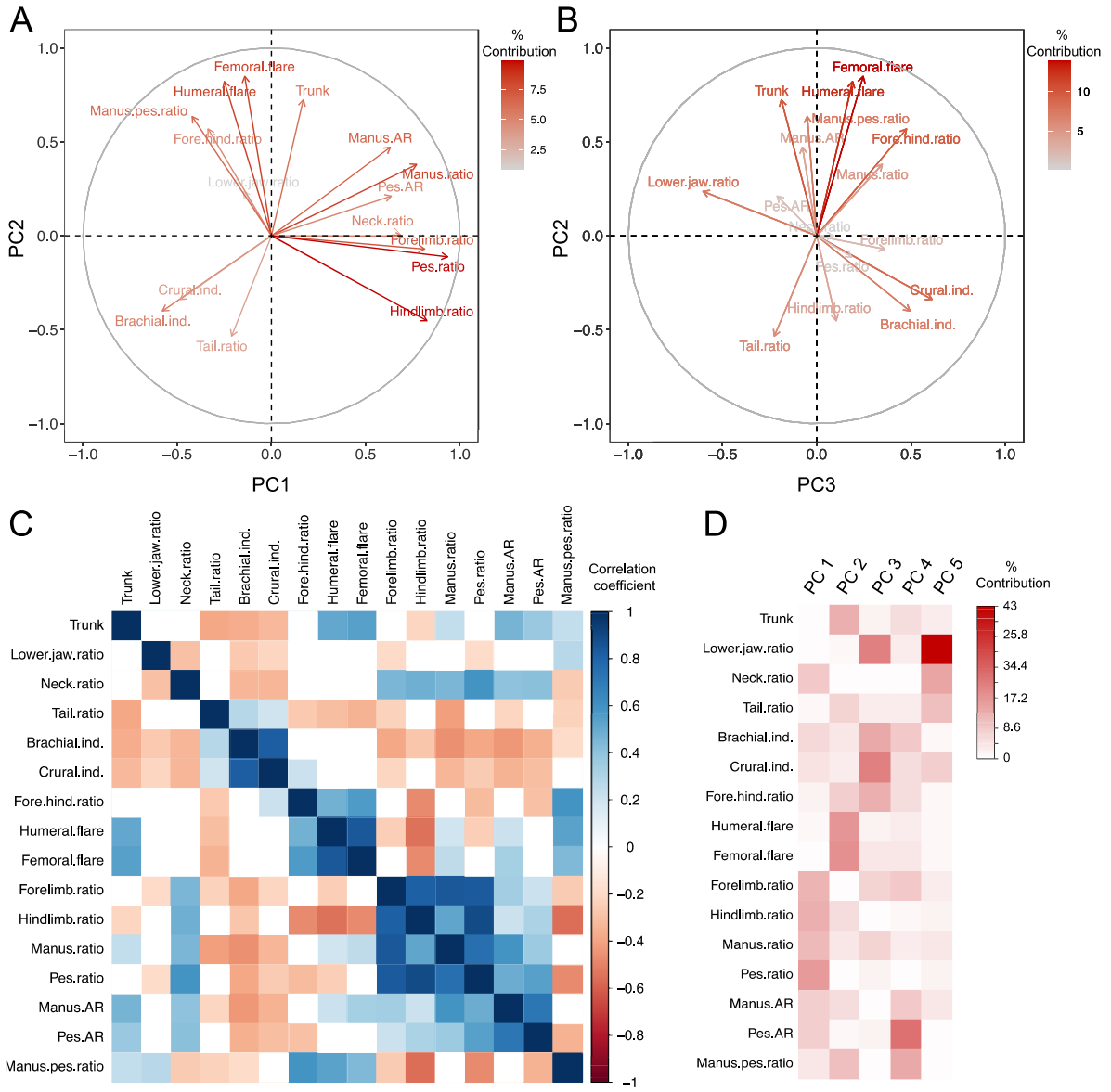

Fig. S3. Character contributions to the locomotory morphospace. (A, B) Plot showing the relative contribution of each character as a colour gradient (grey = low, red = high) as well as the direction in which they affect morphospace PC1–2 (A) and PC2–3 (B). (C) Correlation matrix showing the patterns of covariation between the 16 variables used to build the locomotory morphospace in Mesozoic marine reptiles. Colour has been applied only to statistically significant correlations (Pearson's correlation coefficient, $p < 0.05$), with positive correlation highlighted in blue and negative correlation in red. (D) Relative importance of each functional character to the first 5 axes of variation, which were retained for the disparity calculations and summarise 82% of the total variability.

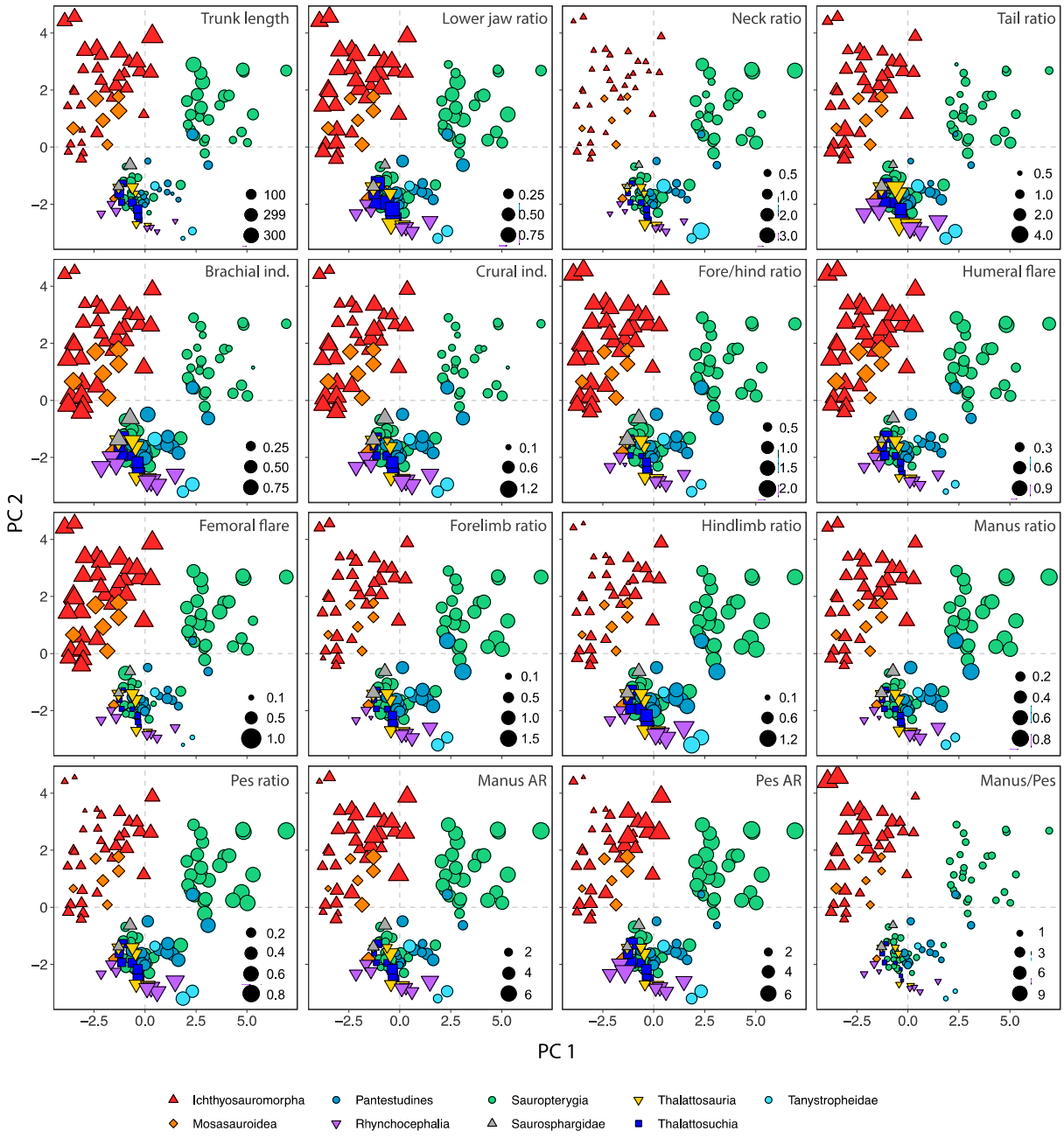

Fig. S4. Character contribution to the locomotory morphospace visualised per taxon. Bidimensional plots of PC1–2, where the point sizes correspond to the relative numerical value of the 16 characters used in the morphospace analysis: trunk length (cm), other functional ratios (no units).

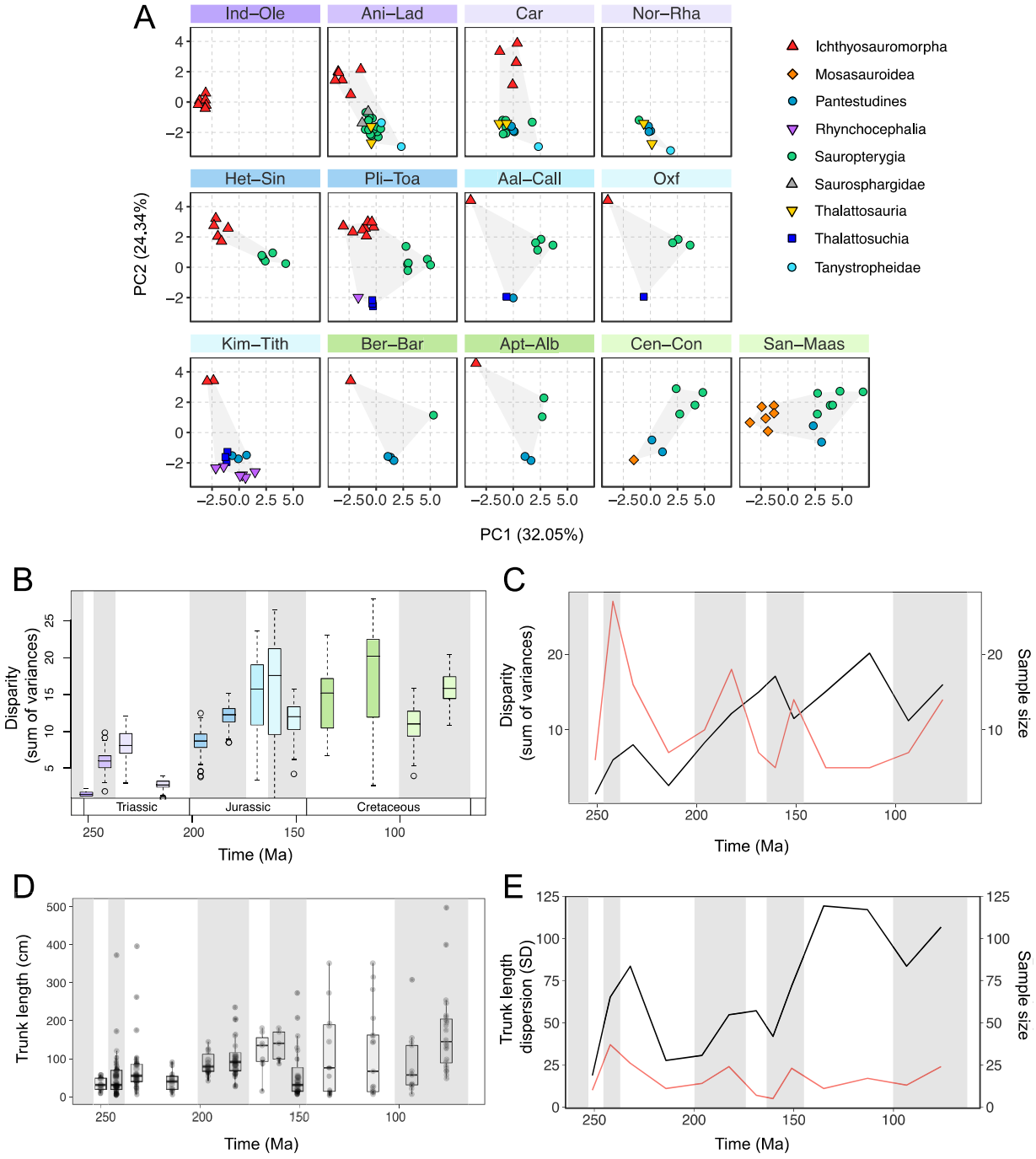

Fig. S5. Time-based analyses of disparity using alternative time intervals. (A) Changes in the main axes of variation PC1 and 2 throughout the Mesozoic using an alternative array of 13 time intervals: Induan–Olenekian, Anisian–Ladinian, Carnian, Norian–Rhaetian, Hettangian–Sinemurian, Pliensbachian–Toarcian, Aalenian–Callovian, Oxfordian, Kimmeridgian–Tithonian, Berriasian–Barremian, Aptian–Albian, Cenomanian–Coniacian and Santonian–Maastrichtian. Alternative analysis to Fig. 3A. (B) Locomotory disparity represented by the sum of variance for Mesozoic marine reptiles for 13 time-bins throughout the Mesozoic. Alternative analysis to Fig. 3D. (C) Locomotory disparity in Mesozoic marine reptiles (black line), calculated as the sum of variances, plotted alongside the sample size for each time bin (red line). Alternative analysis to Fig. 6A. (D) Box plots of trunk length for Mesozoic marine reptiles across 13 Mesozoic time intervals. Alternative analysis to Fig. 5B. (E) Dispersion of trunk lengths in Mesozoic marine reptiles, calculated as the standard deviation (black line) and the sample size for each time bin (red line). Alternative analysis to Fig. 6B.

PC	Eigenvalue	% Cumulative variance
1	5.13	32.05
2	3.89	56.38
3	1.75	67.32
4	1.48	76.57
5	0.90	82.20
6	0.73	86.76
7	0.47	89.72
8	0.40	92.25
9	0.38	94.62
10	0.27	96.32
11	0.24	97.82
12	0.14	98.68
13	0.10	99.29
14	0.06	99.68
15	0.04	99.94
16	0.01	100.00

TABLE S1. Eigenvalues and their contribution to total variance for each principal component axis.
Values are expressed as a percentage relative to total variance and correspond to the main morphospace analysis of Mesozoic marine reptiles.

Analysis	Time bins	Age limits
Total disparity (11 time-bins)	1. Induan-Olenekian	251.9–246.8
	2. Anisian-Ladinian	246.8–237
	3. Carnian	237–228.5
	4. Norian-Rhaetian	228.5–-201.4
	5. Hettangian-Sinemurian	201.4–191.4
	6. Pliensbachian-Toarcian	191.4–174.2
	7. Aalenian-Callovian	174.2–163.1
	8. Oxfordian-Tithonian	163.1–145
	9. Berriasian-Albian	145–100.5
	10. Cenomanian-Coniacian	100.5–86.5
	11. Cenomanian-Maastrichtian	86.5–66
Total disparity (13 time-bins)	1. Induan-Olenekian	251.9–246.8
	2. Anisian-Ladinian	246.8–237
	3. Carnian	237–228.5
	4. Norian-Rhaetian	228.5–-201.4
	5. Hettangian-Sinemurian	201.4–191.4
	6. Pliensbachian-Toarcian	191.4–174.2
	7. Aalenian-Callovian	174.2–163.1
	8. Oxfordian	163.1–157.3
	9. Oxfordian-Tithonian	157.3–145
	10. Berriasian-Barremian	145–126.3
	11. Aptian-Albian	126.3–100.5
	12. Cenomanian-Coniacian	100.5–86.5
	13. Cenomanian-Maastrichtian	86.5–66
Partial disparity	1. Induan-Olenekian	251.9–246.8
	2. Anisian-Ladinian	246.8–237
	3. Carnian-Rhaetian	237–201.4
	4. Hettangian-Toarcian	201.4–174.2
	5. Aalenian-Callovian	174.2–163.1
	6. Oxfordian-Tithonian	163.1–145
	7. Berriasian-Albian	145–100.5
	8. Cenomanian-Maastrichtian	100.5–66
Clade-specific disparity (Ichthyosauromorpha)	1. Induan-Olenekian	251.9–246.8
	2. Anisian-Ladinian	246.8–237
	3. Carnian-Rhaetian	237–201.4
	4. Hettangian-Toarcian	201.4–174.2
	5. Oxfordian-Albian	163.1–100.5
Clade-specific disparity (Sauropterygia)	1. Anisian-Ladinian	246.8–237
	2. Carnian-Rhaetian	237–201.4
	3. Hettangian-Toarcian	201.4–-74.2
	4. Aalenian-Callovian	174.2–163.1
	5. Oxfordian-Tithonian	163.1–145
	6. Berriasian-Albian	145–100.5
	7. Cenomanian-Maastrichtian	100.5–66

TABLE S2. Time intervals used for the disparity analyses.

Comparisons per time-bin	Pairwise *t*-tests		NPMANOVA	
	p-value	Corrected *p*-value	*p*-value	Corrected *p*-value
Triassic/Jurassic	**8.42×10^{-6}**	**2.52×10^{-5}**	**0.001**	**0.003**
Jurassic/Cretaceous	**5.80×10^{-25}**	**1.74×10^{-24}**	**0.019**	0.057
Triassic/Cretaceous	**2.43×10^{-77}**	**7.30×10^{-77}**	**0.001**	**0.003**
Ind-Ole/Ani-Lad	**1.17×10^{-62}**	**1.17×10^{-61}**	**0.001**	0.055
Ani-Lad/Car	**1.00×10^{-14}**	**1.00×10^{-13}**	0.275	1
Car/Nor-Rha	**7.97×10^{-47}**	**7.97×10^{-46}**	0.179	1
Nor-Rha/Het-Sin	**4.24×10^{-77}**	**4.24×10^{-76}**	**0.001**	0.055
Het-Sin/Pli-Toa	**1.01×10^{-43}**	**$1.0^{o} \times 10^{-42}$**	0.634	1
Pli-Toa/Aal-Call	**7.62×10^{-5}**	**0.00076**	0.531	1
Aal-Call/Oxf-Tith	0.9724	1	0.262	1
Oxf-Tith/Ber-Alb	**1.97×10^{-7}**	**1.07×10^{-6}**	0.126	1
Ber-Alb/Cen-Con	**4.46×10^{-25}**	**4.46×10^{-24}**	0.701	1
Cen-Con/San-Maas	**2.15×10^{-30}**	**2.15×10^{-29}**	0.690	1

TABLE S3. Comparative tests for differences in locomotory disparity and morphospace occupation. Pairwise *t*-tests between successive Mesozoic time intervals were applied to test for differences in disparity. Changes in morphospace occupation were assessed using nonparametric multivariate analysis of variance (NPMANOVA). Numbers in bold indicate statistical significance ($p < 0.05$). Corrected and Bonferroni-corrected *p*-values are shown.

Comparisons per time-bin	Variance homogeneity (Ansari-Bradley test)	Two sample group comparisons (Mann-Whitney U test)
Triassic/Jurassic	0.1053	**0.0001**
Jurassic/Cretaceous	**0.0010**	**3.1×10^{-6}**
Triassic/Cretaceous	**0.0041**	**0.0258**
Ind-Ole/Ani-Lad	**0.0663**	0.2926
Ani-Lad/Car	0.7980	**0.0270**
Car/Nor-Rha	0.5219	0.0516
Nor-Rha/Het-Sin	0.9006	**0.0004**
Het-Sin/Pli-Toa	0.3032	0.2338
Pli-Toa/Aal-Call	0.3803	0.1549
Aal-Call/Oxf-Tith	0.4154	**0.0461**
Oxf-Tith/Ber-Alb	**0.0434**	0.1698
Ber-Alb/Cen-Con	**0.0096**	0.6149
Cen-Con/San-Maas	0.8947	0.9985

TABLE S4. Comparative tests for differences in trunk length dispersion and mean trunk length in Mesozoic marine reptiles. Changes in trunk length disparity and the mean trunk length between successive Mesozoic time intervals were assessed using the non-parametric Ansari-Bradley statistical test for variance homogeneity and the Mann-Whitney U test respectively. Numbers in bold indicate statistical significance ($p < 0.05$).

DESCRIPTION OF FUNCTIONAL CHARACTERS

Sixteen continuous characters have been used for this analysis, including a proxy for body size (1), general body proportions (2-4) and functional ratios from the appendicular skeleton (5-16) (Fig 1). Research based on a multivariate analysis including some of these characters has shown to be informative of aquatic locomotion in semiaquatic mammals (Gingerich 2003). Expanding on this approach, a modified list of characters has been elaborated with Mesozoic marine reptiles in mind.

Trunk length

This character represents the longitudinal distance measured along the backbone between the mid-point of the glenoid to the mid-point of the acetabulum, or intergirdle distance. Because regionalisation patterns of the thoracic vertebrae vary depending on the clade, the intergirdle distance represents a good proxy for the trunk and it is functionally equivalent between all groups. Mesozoic marine reptiles and aquatic tetrapods in general show a great disparity of body sizes, ranging from the 5-10 centimetres in some small pachypleurosaurs to the 21 m of the colossal *Shonisaurus*. To date there is no consensus on what the best proxy for body mass is for aquatic animals. Due to the huge variation in body proportions between and within clades, total body length might not be the best suited proxy, and for this reason trunk length has been considered a better option in the past (Buchholtz 2001; O'Keefe 2002; O'Keefe & Carrano 2005). This distance is often used to compare relative measurements of body proportions in fossil (Sander 1989) and living reptiles (Higham *et al.* 2001).

Body size often correlates with aquatic specialisation and locomotion in aquatic animals. In living animals, large sizes are associated with smaller costs of transport during cruising (Fish 2000; Goldbogen 2018), partly due to the reduction in the drag relative to the volume as a result of the scaling effects, as shown in chapters 3 and 4. Large bodies are also associated to the transition to pelagic lifestyle and the acquisition of lift-based swimming modes (Fish 2000). An increase of body size has been well documented in various clades of extant (Gearty *et al.*, 2018) and fossil (Benson *et al.* 2012) aquatic tetrapods.

Lower jaw ratio

This character is a proxy for skull size, calculated as the ratio of the lower jaw (i.e., mandibular length), measured along the ramus, and the trunk length. The skull size is related to the size of maximum gape and therefore the prey size. The proportion of head to body size is an important characteristic of the main body plan and is indirectly linked to locomotion through the connection between foraging habits and hunting style with locomotion (Massare 1988).

Neck ratio

The neck ratio measures the proportion of the length of the neck relative to the trunk. Here, the length of the neck is measured as the distance from the atlas or the base of the skull, to the anterior margin of the pectoral girdle (Sander 1989; Lin & Rieppel 1998). This measure might differ slightly from the length of the cervical series, but it can be more consistently measured between the different clades. For example, in ichthyosaurs atlas and axis are easy to identify, but the subsequent cervical vertebrae grade into trunk vertebrae in shape and dimensions and therefore the neck base is arbitrarily determined by a sudden and rapid change in centrum proportions (Buchholtz 2001; McGowan & Motani 2003). In other cases, the transition between cervical to pectoral or dorsal vertebrae is well defined but it is obscured by taphonomic effects, erosion, or orientation of the fossil. Using a definition of the neck as a region instead as a series of cervical vertebrae helps to overcome these ambiguities.

Neck ratio is very variable within aquatic fossil reptiles and shows a great plasticity particularly in some groups such as Sauropterygia (Soul & Benson 2017), Thalattosauria (Druckenmiller *et al.* 2020) and the protorosaurian tanystropheids (Jaquier *et al.* 2017). The neck ratio has been associated with trophic ecology in various clades (Zammit *et al.* 2008; Anquetin *et al.* 2017), but it can potentially affect the drag-associated costs of swimming, as has been shown in chapter 4. Additionally, long necks might influence body stability through the displacement of the centre of gravity (Henderson 2006).

Tail ratio

The tail length was calculated as the distance, measured along the backbone, between the mid-point of the acetabulum and the tip of the tail. This is then divided by the trunk length to calculate the tail ratio. A proportionately long tail is usually a primitive condition in many groups of reptiles. Semiaquatic animals of distant clades that swim by undulation use their long, often flattened tails to generate thrust. In the transition to lift-based modes of aquatic locomotion, there is often a reduction of the tail, particularly marked in underwater fliers in which the tail becomes a stabiliser or rudder (Fish & Lauder 2017).

Brachial index

This metric represents the proportion of epipodial to propodial length in the forelimb. It is calculated as the length of the radius divided by the humeral length, where the radius and humeral length are measured as the distance between the proximal and distal articular surfaces or each bone. The brachial index is a measure of the outlever/inlever ratio of the forelimb, and it correlates with the out-velocity in terrestrial animals (Croft & Anderson 2008). Semiaquatic taxa display higher values of brachial index than more aquatically adapted animals due mainly to a shortening of the radius (Caldwell 2002).

Crural Index

Crural index is calculated as the length of the tibia divided by the femoral length, where the tibial and femoral length are measured as the distance between the proximal and distal articular surfaces of each bone. Both brachial and crural indices are used here to quantify the relative distal limb elongation which is correlated with cursoriality (Young *et al.* 2014). As in the brachial index, crural index is reduced with increasing aquatic adaptation as the epipodial bones become relatively shorter compared to the propodials (Caldwell 2002).

Ratio of forelimb to hindlimb

This ratio is calculated as the length of the humerus divided by the length of the femur. It reflects differences in length between the forelimb and hindlimb and can contribute to distinguishing transitions towards axial swimming in contrast to appendicular swimming. A marked reduction of the hindlimbs and loss of mobility is usually observed in the clades evolving caudal oscillatory locomotion, leading sometimes to their complete loss as is the case in cetaceans and sirenians (Reidenberg 2007). This relative reduction is not observed in specialist appendicular swimmers for which the hindlimbs function as rudders and stabilisers as seen in bipedal underwater fliers (Fish & Lauder 2017; Mayerl *et al.* 2017) or as propellers in the case of quadrupedal underwater fliers like plesiosaurs (Muscutt *et al.* 2017).

Humeral flare

This ratio describes the relationship between the main humeral axis and the degree of distal expansion. It is calculated as the maximum distal width of the humerus divided by the total humeral length. An expansion of the distal portion of the humerus along with a shortening of the humeral epiphysis, resulting in an increase of this ratio, are correlated with adaptation in aquatic locomotion in semiaquatic mammals (Gingerich 2003; Botton-Divet *et al.* 2017), cheloniids (Rivera & W. Blob 2010) and cetaceans (Fish 1996; Cooper *et al.* 2007).

Femoral flare

This ratio describes the relationship between the main femoral axis and the degree of distal expansion. It is calculated as the maximum distal width of the femur divided by its total length. In secondarily aquatic mammals, a robust, short and distally expanded femur is also associated with aquatic specialisation (Gingerich 2003) and the transformation of hindlimbs into flippers (Adam 2009).

Forelimb ratio, hindlimb ratio, manus ratio and pes ratio

The forelimb and hindlimb are calculated as the total limb length, measured from the proximal propodial end to the distal end of the longest digit, divided by the trunk length. The manus

and pes ratios are calculated as the autopodial length, measured from the proximal-most end of the mesopodial bones to the end of the longest digit, divided by the trunk.

These four characters describe the main limb proportions in relation to body size. Limbs and autopodia become proportionally large in specialised appendicular swimmers relative to more terrestrially adapted forms (Rivera *et al.* 2013) and also relative to axial swimmers. Elongated autopodia are often observed in very derived aquatic animals as a result of hyperphalangy (Caldwell 2002; Berta *et al.* 2006; Cooper *et al.* 2007) or phalangeal elongation (Berta *et al.* 2006; Rivera *et al.* 2013).

Manus and pes aspect ratio

The aspect ratio of both autopodia (manus and pes) are taken as a proxy for the paddle/flipper aspect ratio. High aspect ratio in control and propulsive surfaces is correlated with reduction of the induced drag (Hoerner 1965; Hoerner & Borst 1985) and high hydrodynamic efficiency (i.e., lift/drag proportion) (Fish 2000, 2004; Weber *et al.* 2009).

Here, aspect ratio was calculated as the square of the span divided by the planar area (autopodium length^2/autopodium area), as done in flippers and flukes of aquatic animals (Weber *et al.* 2009, 2014). Only the autopodium is considered because flippers have varying configurations depending on the group which involve different bones of the limb, but the manus and the pes are always part of the flipper and contribute to most of its area. The manus and pes areas were taken from scaled photographs of articulated autopodia in dorsal view using the program Fiji (Schindelin *et al.* 2012). For that, the planar form was delimited by a polygon following the tips of the digits and the bases of the mesopodial bones.

Manus/pes ratio

This ratio is calculated by dividing the manus area by the pes area. A reduction of the pes area relative to the manus is observed in some very specialised caudal oscillators such as ophthalmosaurid ichthyosaurs (Moon & Kirton 2016, 2018). Expanded feet are present in hindlimb rowers, quadrupedal underwater fliers and they can raise manoeuvrability when they are used as rudders (Fish 2004).

INFERENCE OF MISSING DATA

Triassic Sauropterygia

Lariosaurus xingyiensis

Nothosauroidea

Distal phalangeal elements are missing from the manus and pes from the specimen IVPP V11866 (Rieppel *et al.* 2003). The manus was reconstructed from XNGM WS-30-R19, another specimen of *Lariosaurus xingyiensis* (Lin *et al.* 2017). The missing elements of the pes were inferred from the foot of *Nothosaurus youngi* (WS-30-R24), another species of nothosauroid from the Xingyi fauna that has been shown to have a postcranial anatomy close to *Lariosaurus* (Ji *et al.* 2014).

Neusticosaurus edwardsi

Pachypleurosauria

The missing manus in the specimen PIMUZ T3935 was inferred from another specimen of the same species, PIMUZ T3460 which has a complete one.

Nothosaurus giganteus

Nothosauroidea

Most of the forelimb phalanges are missing in the otherwise complete specimen PIMUZ T4829. The hands of *Nothosaurus youngi*, the closest relative with fully preserved limbs, were used to infer these missing elements, using the epipodials as scaling element. *N. youngi* has more gracile hands than *N. giganteus*, but the main proportions are maintained.

Paraplacodus broilii

Placodontia

PIMUZ T4755 is an almost complete skeleton only missing part of the rostrum and the distal elements of the hindlimb which has been described in great detail (Rieppel 2000). The length of the lower jaw was inferred from PIMUZ T4774, a specimen of the same species that includes a disarticulated set of postcrania and complete lower portion, including a humerus, femur and other girdle elements very close in size to PIMUZ T4755. The missing elements of the pes were inferred based on *Placodus inexpectatus* GMPKU-P-1054 (Jiang *et al.* 2008), a closely related basal member of Placodontia with complete limbs (Wang *et al.* 2018). Although the limbs of *Placodus* are more gracile than those of *Paraplacodus*, both taxa display similar limb proportions as shown by their brachial and crural indexes. *Placodus inexpectatus* was hence used to infer the missing measurements. The left manus of PIMUZ T4755 is fairly complete, with five metacarpals and a minimum of nine phalanges preserved, but the elements have shifted from their places. The right forelimb of *Placodus inexpectatus* (GMPKU-P-1054), was mirrored and scaled to the same humeral length, serving as a

template to rearrange the existing nine phalanges and complete the missing ones assuming a minimal plesiomorphic phalangeal formula of 2-3-4-5-3.

Psephochelys polystoderma

Placodontia

The recently described specimen EBGL009 (Wang *et al.* 2019) is mostly complete and articulated, with beautifully preserved hindlimbs, but the manus are missing. YIGMR TR00005 (Xiaofeng *et al.* 2008) another *P. polystoderma* specimen, with complete although poorly prepared manus, was used to infer the missing measurements by using the humerus as scaling element.

Psephoderma alpinum

Placodontia

Two relatively complete specimens of this species are available, (i) ST82003, described in great detail (Renesto & Tintori 1995) and (ii) MSNM V 527, a smaller specimen housed in the Museo Civico di Historia Naturale of Milan. Unfortunately, none of them preserves the full forelimbs. *Psephochelys polystoderma* the sister taxon to this species (Neenan *et al.* 2015; Wang *et al.* 2018) was used to infer the missing forelimb elements in ST82003, the largest and most complete of the two specimens, which was finally used in this study.

Sinocyamodus xinpuensis

Placodontia

IVPP V 17051 is a practically complete adult specimen of *Sinocyamodus xinpuensis* (Wang *et al.* 2018). The right hand preserves a few mesopodial bones and phalanges in disarray. The limb measurements were inferred from the complete forelimb of the holotype (IVPP V11872; images by S. Zhang), a subadult specimen.

Jurassic and Cretaceous Sauropterygia (Plesiosauria)

The total length of the autopodium in plesiosaurs is measured following digit III, which is the longest in both hand and pes. The length of phalanges decreases with a ratio of phalange n/ phalange n+1 from proximal to distal. Missing phalanges were estimated by multiplying the length of the distalmost preserved phalanx by this ratio, estimated from the preserved phalanges.

The number of phalanges in digit III is variable across Plesiosauria. Based on well-preserved specimens, the following minimum numbers of phalanges in digit III were assumed for each group: eight for basal plesiosaurians, rhomaleosaurids and basal pliosaurids, 11 for microcleidids, 11 for leptocleidids, 13 for cryptocleidids, 12 for elasmosaurs other than *Styxosaurus* and 12 for polycotilids. *Styxosaurus* is an exception within elasmosaurs, with 17–18 phalanges preserved in various specimens (e.g., SDSM 451, NJSM 15435).

Albertonectes vanderveldei

Elasmosauridae

The full length of the right paddle in TMP 2007-011.000 was reconstructed by adding five extra phalanges to make a total of 12 in digit III. In the hindlimb, most phalanges are missing, and the length of the pes was thus inferred using the ratio of manus/pes length calculated from the elasmosaurin elasmosaur *Terminonatator ponteixensis* (RSM P2414.1; photographs by R. McKellar and E. Bamford from the Royal Saskatchewan Museum).

Attenborosaurus conybeari

Pliosauridae

The hindlimbs of NHMUK R1339 only preserve the femur. The dimensions of the missing elements (tibia and pes) were inferred by averaging estimations from two related Early Jurassic pliosaurs, *Thalassiodracon hawkinsi* (NHMUK 2020) and *Hauffiosaurus zanoni* (Hauff. uncat), with femur as scaling element.

Hauffiosaurus zanoni

Basal Pliosauridae

(Hauff. Uncat). The front left paddle and right rear paddle are the more complete, with six and five phalanges preserved in digit III (Vincent 2011). A total of eight phalanges in digit III were assumed in both limbs to infer the measurements.

Hydrotherosaurus alexandrae

Elasmosauridae

The left pelvic paddle in UCMP 33912 is the most complete, although elements are not in full articulation. Welles (1943) estimated that there were at least 11 phalanges in the digit II. Here, the length of the rear paddle was inferred by realigning digitally the phalanges on digit III and adding one to complete an assumed number of 12 in digit III. Almost no phalanges are preserved from the front paddle. The length of the manus was thus inferred using the average ratio of manus/pes length calculated from the elasmosaurid *Styxosaurus* sp., SDSM 451 (Welles & Bump 1949) and *Terminonatator ponteixensis*, RSM P2414.1(photographs by R. McKellar and E. Bamford from the Royal Saskatchewan Museum).

Libonectes atlasense

Elasmosauridae

A few distal elements are missing from both the fore and hind paddles of SMNK-PAL 3978 (Sachs & Kear 2017). Measurements were inferred assuming a total 12 phalanges in digit III.

Morenosaurus stocki

Elasmosauridae

LACM/CIT 2802 preserved an almost complete and articulated fore paddle, with seven phalanges in digit III. The manus dimensions were inferred after adding five more phalanges to make a total of 12. Only a few elements of the pes are preserved in this specimen. The dimensions of the missing elements were inferred from a closely related wedellonectian, *Afrosaurus furlongi* LACM 2748 (O'Gorman 2019), in which the pes is completely preserved.

Muraenosaurus leedsi

Cryptoclididae

Measurements for this species were taken from various specimens housed in the Natural History Museum of London. Main body proportions and length of long bones were an average of measurements from NHMUK 2678, NHMUK 2421 and NHMUK 2863, three incomplete specimens of very similar size (Andrews 1910). The manus and pes dimensions were inferred from the complete limbs of a smaller specimen, NHMUK 2864, using the humerus and femur as scaling elements respectively.

Rhomaleosaurus cramptoni

Rhomaleosauridae. Basal Plesiosauria

NMING F8785 is a mostly complete specimen, but it has an artificial arrangement of the phalanges (Smith 2007). The autopodial dimensions were inferred from OUMNH-PAL-J66986, a juvenile specimen of the closely related species *Rhomaleosaurus zetlandicus* (photographs by H. Ketchum, from the Oxford University Museum of Natural History).

Rhomaleosaurus megacephalus

Rhomaleosauridae.

Historic photographs were used to extract the measurements from BRSMG Cb2335, the holotype of *R. megacephalus* lost during the Bristol raid in World War II (Smith 2007, 2015). Missing distal elements in the front and rear paddles were reconstructed to a total of eight phalanges in digit III.

Thalassomedon hanningtoni

Elasmosauridae

The hindlimb of DMNH 1588 is fully preserved and articulated, with 12 phalanges in digit III, but the forelimb is only represented by the left humerus, radius and ulna (Welles 1943). The missing manus was inferred from the almost complete left pectoral paddle of FMNH 12009, the holotype of *Alzadasaurus riggsi* (Welles 1962), a synonym of *Thalassomedon haningtoni* (Carpenter

1999). This fossil has eight phalanges preserved in the 3rd digit, and thus four more were added to make a total of 12.

Ichthyosauromorpha

Caypullisaurus bonapartei

Ophthalmosauridae

The missing hindlimb of the holotype MAC-N-32 (Fernández 1997), was inferred from MLP 83-XI-16-1 (Fernández 2007), a slightly smaller specimen of the same species which preserves the proximal part of a forelimb, part of the pectoral girdle and a complete hindlimb using the humerus scaling element. The distal part of the caudal series is also missing in MAC-N-32. The tail proportions were inferred from the lost holotype of *Platypterygius platydactylus* (Broili 1907), the only closest relative of which there is an account of an almost complete vertebral series in the literature.

Cryopterygius kristianseae

Ophthalmosauridae

Most of the tail is present in the holotype PMO 214.578 (Druckenmiller *et al.* 2012) but the postflexural vertebrae are missing. The remaining end part of the tail was inferred using the postflexural-to-total caudal length from *Ophthalmosaurus icenicus* (GPIT/RE/9410, personal observation), a close ophthalmosaurine relative. The hindlimb is practically complete, including the pes, but this is distorted and partially obscured by other bones. Its dimensions were also inferred from GPIT/RE/9410, using the femur as scaling element.

Eretmophis carroldongi

Hupehsuchia

The holotype, WGSC V26020 is a fairly complete specimen only missing the head and neck (Chen *et al.* 2015). The lower jaw and head proportions were estimated from a recently described specimen, YAGM V 1401 (Cheng *et al.* 2019).

Hupehsuchus nanchangensis

Hupehsuchia

The tail in the holotype IVPP V3232 is missing the distalmost elements. Tail proportions were inferred from ZMNH M8127, a smaller specimen (Wu *et al.* 2016).

Ichthyosaurus larkini

Ichthyosauridae

The holotype of this species is an almost complete specimen (BRSUG 25300), only missing the distal end of both pedes (Lomax & Massare 2017). The missing elements were inferred from a referred specimen of the same species, AGC 11 (Lomax & Massare 2017).

Leptonectes tenuirostris

Leptonectidae

M3564 is a practically complete specimen housed in the National Museum of Wales, missing only the post-flexural vertebrae. The missing portion of the tail was inferred from a smaller specimen, NHMUK R498 (McGowan 1974).

Phalarodon atavus

Mixosauridae

The cervical vertebrae, as well as various proximal hindlimb elements (i.e., tibia and carpals) are missing in the holotype LPV 30872 (Liu *et al.* 2013*b*). The neck proportion was inferred from the holotype of *Phalarodon callawayi*, CMC VP 7275 (Schmitz *et al.* 2004). The hindlimbs were reconstructed on the basis of PMU R 188, a referred specimen of *P. callawayi* (Merriam 1911).

Platypterygius hercynicus

Ophthalmosauridae

The SGS specimen (housed at the Städtisches Museum Schloss Salder, Salzgitter, Germany) is the holotype of *P. hercynicus*. Presently it is the most complete *Platypterygius* specimen after the loss during World War II of the holotype of *P. platydactylus*, the type species of *Platypterygius* (Fischer 2012). The SGS specimen misses less than half of the distal caudal vertebrae and the hindlimbs. These were inferred based on the detailed account and diagrams made by Broili (1907) of the lost holotype of *P. platydactylus*.

Shonisaurus popularis

Shastasauridae

Measurements were taken from the detailed reconstruction presented by Camp (1980) based on various specimens of *Shonisaurus popularis*. The main body proportions were based on the fairly complete specimen A-5. The lower jaw measurement was based on the reconstructed skull, based on fragments from five specimens. The dimensions of the fore paddles have been taken from the almost complete limbs of specimen B, restored by Camp (1980).

Utatsusaurus hatai

Basal Eoichthyosauria

The holotype IGPS 95941 comprises the greatest portion of a torso, forelimbs, neck and head (Motani 1997). The body proportions missing in the holotype were taken from the composite reconstruction by Motani (1998) based on multiple specimens. Measurements of the manus were taken from a detailed forelimb reconstruction by Motani (1997) based on IGPS 95941 and the paratype IGPS 95942. Measurements of the femur and tibia were taken from specimen E described by Shikama *et al.* (1978), assuming equal dimensions of humerus and femur (Shikama *et al.*, 1978; Motani, 1998). The pes was inferred from the basal grippidian *Gulosaurus helmi* (TMP 89.127.5), originally described as *Grippia longirostris* (Brinkman & Nicholls 1992). Grippidians, which show a forelimb configuration similar to *Utatsusaurus* (Motani 1997), are recovered as being phylogenetically close to *Utatsusaurus* at the base of Eoichthyosauria (Moon 2017).

Mosasauroidea

Aigialosaurus buchichi

Aigialosauridae, Mosasauroidea

Measurements of the tail, which is incomplete in NMW, the holotype of *Aigialosaurus buchichi* were taken from the reconstruction made by Carrol & Debraga (1992).

Clidastes propython

Mosasaurinae, Mosasauridae

The specimen KUVP 1022 (Williston & Case, 1892) is a beautifully preserved skeleton missing the pes - except for one carpal and one metacarpal - and a few distal phalanges in the forelimb. The manus measurements were inferred from the specimen YPM 24938 of *Clidastes sp* (Russell 1967). The missing pes was inferred from AMNH 1513, the holotype of *Clidastes tortor*, a synonym of *C. propython* (Russell 1967; Lively 2018), of which complete forelimbs and partial hindlimbs are known (Sternberg 1909).

Halisaurus sternbergii (sin. *Eonatator sternbergii*)

Halisaurinae, Mosasauroidea

PMU R163 is a practically complete specimen only missing the pes and distal phalangeal elements of the forelimb (Bardet & Pereda Suberbiola 2001). The pes proportions were inferred from the closely related Colombian halisaurine *Eonatator coellensis* (IGM-P881237) (Páramo-Fonseca 2014) using the femur as scale. The length of the hand was inferred based on IGM-P881237, which preserves the longest digit using the humerus as scaling element. A minimum planform area was calculated constrained by the length of the longest digit and the remaining preserved metacarpals.

*Mosasaurus lemonnieri (*cf. *conodon)*

Mosasaurinae, Mosasauridae

IRSBN 3119 preserves the skull, an almost complete vertebral series, and a great part of the limbs. In this specimen the jaw is broken and about half of it is missing, but the upper part of the skull is complete from the tip of the rostrum to the occipital condyle. This allowed us to infer this measurement from R28, another *M. lemonnieri* specimen with a complete skull. The missing distal limb elements were inferred from SDSM 252, a specimen of *Mosasaurus conodon* (Russell 1967), using the propodials as scale.

Plotosaurus bennisoni

Mosasaurinae, Mosasauridae

Measurements were taken from the detailed osteological study and skeletal restoration previously published (Lindgren *et al.* 2007, 2008), based on various UCPM and CIT specimens of *P. benisonni*.

Pantestudines

Eurysternum wagleri

Eurysternidae, Cryptodira

IGPS 651 is a complete skeleton preserved in dorsal view, which means that only the distal part of the humerus is visible. The humeral length was inferred from BSPG 1960 VIII 43, another *Eurysternum wagleri* specimen (Anquetin & Joyce 2014).

Hoyasemys jimenezi

Sinemydidae, Cryptodira

The tail in MCCM−LH 84 (Pérez-García *et al.* 2012) is incomplete. The average tail ratios from various specimens of closely related sinemydids was used to infer the full length of the tail: *Jeholochelys lingyuanensis* (PMOL-AR00211, PMOL-AR00213, Zhou & Rabi, 2015), *Ordosemys liaoxiensis* (GM V3001, Tong *et al.*, 2004) and *Sinemys brevispinus* (IVPP V1034 (Tong & Brinkman 2013)

Platychelys oberndorferi

Platychelyidae, Panpleurodira

The humerus and femur are not completely visible in this specimen because it is preserved in dorsal view. These measurements were inferred from another closely related platychelyid *Notoemys laticentralis* MOZ-P-4040 (Fernandez & de la Fuente 1993).

Rhinochelys nammourensis

Protostegidae, Chelonidoidea, Cryptodira

The neck and head missing in the specimen ESC-2 (Tong *et al.* 2006) where inferred from a smaller specimen MM V3933 of *R. nammourensis* (Tong *et al.* 2006). The femur and tibia, which are not entirely visible in ESC-2, were inferred from the closely related protostegid *Desmatochelys lowii* (López-Conde, 2019)

Xinjiangchelys wusu

Xinjiangchelyidae, Pancryptodira

Missing phalanges of pedal digit V were reconstructed assuming the formula 2-3-3-3-3 of xinjiangchelyids (Shao *et al.* 201820). The missing tail was inferred using the average tail ratio from various specimens of Sinemydidae, the sister taxon of Xinjiangchelyidae (Shao *et al.* 2018): *Jeholochelys lingyuanensis,* PMOL-AR00213 (Shao *et al.* 2018); *Ordosemys liaoxiensis,* GM V3001 (Tong *et al.* 2004) *and Liaochelys,* PMOL-AR00160 (Zhou 2010). The distal width of the humerus, which is not exposed in any of the PMOL-SGP specimens (Rabi *et al.* 2013) was inferred from *Xinjiangchelys rediplicatoides* IVPP 9539 (Brinkman *et al.* 2013).

Thalattosuchia

Cricosaurus suevicus

Metriorhynchoidea

The distal elements hands and pes in SMNS 9808 are preserved in disarray. Measurements of the manus were taken from the reconstructed forelimb by Fraas (1902).

Pelagosaurus typus

Teleosauroidea

Most of the manus is missing in SMNS 52034. Measurements were taken from a forelimb reconstruction based on various *P. typus* specimens UH 4, UH 8, SMNS 80066, and NHMUS M 62 2516 (Mueller-Töwe 2006), using the humerus as scale.

Steneosaurus bollensis

Teleosauroidea

Measurements for the missing hand in SMNS 54063 were inferred from GPIT/RE/1193 2, a large specimen of *S. bollensis,* using the humerus as scale.

Thalattosauria

Clarazia schinzii

Thalattosauroidea, Thalattosauria

The missing humerus in the specimen PIMUZ A/III 211 was inferred based on the average proportion of humerus/trunk in various closely related species of thalattosaurid thalattosaurs, *Xinpusaurus suni*, Gmr-010 (Liu 2013); *Concavispina bisiridens*, ZMNH M8804 (Liu *et al.* 2013*a*); and *Gunakadeit joseeae*, UAMES 23258 (Druckenmiller *et al.* 2020). The phalanges in the manus of PIMUZ A/III 211 are slightly displaced. These were reordered and a few extra distal elements added assuming the same phalangeal formula 2-3-4-5-3, as in *Xinpusaurus suni* (Liu 2013).

Saurosphargidae

Helveticosurus zollingeri

PIMUZ T4352 is a very complete specimen, missing some distal phalangeal elements of the manus and lacking the distal caudal vertebrae. The forelimb was measured along digit IV, the most complete with six phalanges. A minimum area for the hand was measured by adding one extra phalanx to each of digits I-III to match the number of phalanges in the pes. A minimum tail length was inferred from the closely related species *Eusaurosphargis dalsassoi* (Scheyer *et al.* 2017).

Largocephalosaurus qianensis

In the holotype IVPP V 15638 (Li *et al.* 2013), most of the distal elements from manus and pes are missing. The manus was inferred from GMPKU-P-1532-B, a referred specimen of the same species (Li *et al.* 2013). The pes was inferred from WIGM SPC V 1009, a specimen of the closely related species *Largocephalosaurus polycarpon* (Cheng *et al.*, 2012 and photographic material).

Tanystropheidae

Dinocephalosaurus orientalis

The missing tail of *D. orientalis* IVPP 13898 (Rieppel *et al.*, 2008) was inferred as an average from various specimens of closely related tanystropheids: *Tanystropheus* sp. (MSNM BES SC 265, PIMUZ T 2818) and *Tanytrachelos ahynis* (YPM 7491). A few distal phalanges are missing in both fore and hindlimb. These were inferred considering a minimum phalangeal count as in *Tanystropheus*: 1-2-3-4-1 (hand) and 2-3-4-4-3 (pes).

Tanystropheus longobardicus

Most measurements and proportions were taken from the large specimen PIMUZ T 2128 (personal observation). In this specimen, most hand phalanges are missing, and the pes is lacking the

most distal ones. Manus and pes measurements were inferred from PIMUZ T 2817, another *T. longobardicus* specimen (Wild 1980; Nosotti 2007).

Tanytrachelos ahynis

The incomplete tail in the specimen YPM 7622 was inferred from YPM 7491, belonging to the same species. The missing lower jaw in YPM 7622 was inferred from the skull reconstruction by Olsen (Olsen 1979) based on the referred specimen YPM 7402.

Rhynchocephalia

Kallimodon pulchellus

Sapheosauridae

The incomplete tail of the specimen SNSB-BSPG 1887 VI 1 was inferred from the co-specific specimen Rhy 2 (Cocude-Michel 1963)

Palaeopleurosaurus posidoniae

Length of the tail in SMNS 50722 (Carroll 1985) is an average from inferred lengths based on the closely related species *Pleurosaurus ginsburgi*, MNHN 1983-4 CNJ 67 (Fish 2000; Berta *et al.* 2006) (Dupret 2004), and *Vadasaurus herzogi*, AMNH FARB 37268 (Bever & Norell 2017).

Pleurosaurus goldfussi

The tip of the tail is missing in MNNL 15640 (Cocude-Michel 1963). This measurement was inferred from an average of specimens at the Museum Eichstatt and Painten (Germany, photographs by S. Sachs).

SUPPLEMENTARY REFERENCES

ADAM, P. J. 2009. Hind limb anatomy. *In* PERRIN, W. F., WÜRSIG, B. and THEWISSEN, J. G. M. (eds.) *Encyclopedia of Marine Mammals*, Academic Press, London, 562–565 pp.

ANDREWS, C. W. 1910. *A descriptive catalogue of the marine reptiles of the Oxford clay, Part I*. British Museum (Natural History), London.

ANQUETIN, J. and JOYCE, W. G. 2014. A reassessment of the Late Jurassic turtle *Eurysternum wagleri* (Eucryptodira, Euristernidae). *Jounal of Vertebrate Paleontology*, **34**, 1317–1328.

ANQUETIN, J., TONG, H. and CLAUDE, J. 2017. A Jurassic stem pleurodire sheds light on the functional origin of neck retraction in turtles. *Scientific Reports*, **7**, 1–10.

BARDET, N. and PEREDA SUBERBIOLA, X. 2001. The basal mosasaurid *Halisaurus sternbergii* from the Late Cretaceous of Kansas (North America): a review of the Uppsala type specimen. *Comptes Rendus de l'Académie des Sciences - Series IIA - Earth and Planetary Science*, **332**, 395–402.

BENSON, R. B. J., EVANS, M. and DRUCKENMILLER, P. S. 2012. High diversity, low disparity and small body size in plesiosaurs (Reptilia, Sauropterygia) from the Triassic–Jurassic boundary. *PLoS ONE*, **7**, e31838.

BERTA, A., SUMICH, J. L. and KOVACS, K. M. 2006. Pinniped evolution and systematics. *In Marine Mammals: Evolutionary Biology*, Elsevier, San Diego, CA, 27–50 pp.

BEVER, G. S. and NORELL, M. A. 2017. A new rhynchocephalian (Reptilia: Lepidosauria) from the Late Jurassic of Solnhofen (Germany) and the origin of the marine Pleurosauridae. *Royal Society Open Science*, **4**, 170570.

BOTTON-DIVET, L., CORNETTE, R., HOUSSAYE, A., FABRE, A.-C. and HERREL, A. 2017. Swimming and running: a study of the convergence in long bone morphology among semi-aquatic mustelids (Carnivora: Mustelidae). *Biological Journal of the Linnean Society*, **121**, 38–49.

BRINKMAN, D. B. and NICHOLLS, E. L. 1992. A primitive ichthyosaur from the Lower Triassic of British Columbia, Canada. *Palaeontology*, **35**, 465–474.

BRINKMAN, D. B., EBERTH, D. A., XU, X., CLARK, J. M. and WU, X.-C. 2013. Turtles from the Jurassic Shishugou Formation of the Junggar Basin, People's Republic of China, with comments on the basicranial region of basal Eucryptodires. *In* BRINKMAN, D. B., HOLROYD, P. A. and GARDNER, J. D. (eds.) *Morphology and Evolution of Turtles*, Springer Netherlands, Dordrecht, 147–172 pp.

BROILI. 1907. Ein neuer *Ichthyosaurus* aus der norddeutschen Kreide. *Paleontographica*, **54**, 69–138.

BUCHHOLTZ, E. A. 2001. Swimming styles in Jurassic ichthyosaurs. *Journal of Vertebrate Paleontology*, **21**, 61–73.

CALDWELL, M. W. 2002. From fins to limbs to fins: Limb evolution in fossil marine reptiles. *American Journal of Medical Genetics*, **112**, 236–249.

CAMP, C. L. 1980. Large ichthyosaurs from the Upper Triassic of Nevada. *Palaeontographica Abteilung A*, **170**, 139–200.

CARPENTER, K. 1999. Revision of North American elasmosaurs from the Cretaceous of the Western Interior. *Paludicola*, **2**, 148–173.

CARROLL, R. L. 1985. A pleurosaur from the Lower Jurassic and the taxonomic position of the Sphenodontida. *Paleontographica Abteilung A*, **189**, 1–28.

CARROLL, R. L. and DEBRAGA, M. 1992. Aigialosaurs: mid-Cretaceous varanoid lizards. *Journal of Vertebrate Paleontology*, **12**, 66–86.

CHEN, X., MOTANI, R., CHENG, L., JIANG, D. and RIEPPEL, O. 2015. A new specimen of Carroll's mystery hupehsuchian from the Lower Triassic of China. *PLoS ONE*, **10**, 1–15.

CHENG, L., CHEN, X., ZENG, X. and CAI, Y. 2012. A new eosauropterygian (Diapsida: Sauropterygia) from the Middle Triassic of Luoping, Yunnan Province. *Journal of Earth Science*, **23**, 33–40.

CHENG, L., MOTANI, R., JIANG, D., YAN, C., TINTORI, A. and RIEPPEL, O. 2019. Early Triassic marine reptile representing the oldest record of unusually small eyes in reptiles indicating non-visual prey detection. *Scientific Reports*, **9**, 1–11.

COCUDE-MICHEL, M. 1963. Les rhynchocéphales et les sauriens des calcaires lithographiques (Jurassique supérieur) d'Europe occidentale. *Publications du musée des Confluences*, **7**, 3–224.

COOPER, L. N., DAWSON, S. D., REIDENBERG, J. S. and BERTA, A. 2007. Neuromuscular anatomy and evolution of the cetacean forelimb. *The Anatomical Record: Advances in Integrative Anatomy and Evolutionary Biology*, **290**, 1121–1137.

CROFT, D. A. and ANDERSON, L. C. 2008. Locomotion in the extinct notoungulate *Protypotherium*. *Palaeontologia Electronica*, **11**, 1–20.

DRUCKENMILLER, P. S., HURUM, J. H., KNUTSEN, E. M. and NAKREM, H. A. 2012. Two new ophthalmosaurids (Reptilia: Ichthyosauria)- from the Agardhfjellet Formation (Upper Jurassic: Volgian/Tithonian),- Svalbard, Norway. *Norwegian Journal of Geology*, **92**, 311–329.

DRUCKENMILLER, P. S., KELLEY, N. P., METZ, E. T. and BAICHTAL, J. 2020. An articulated Late Triassic (Norian) thalattosauroid from Alaska and ecomorphology and extinction of Thalattosauria. *Scientific Reports*, **10**, 1746.

DUPRET, V. 2004. The pleurosaurs: anatomy and phylogeny. *Revue de Paléobiologie, Genève*, **9**, 61–80.

FERNÁNDEZ, M. 1997. A new ichthyosaur from the Tithonian (Late Jurassic) of the Neuquén Basin, Northwestern Patagonia, Argentina. *Journal of Paleontology*, **71**, 479–484.

FERNANDEZ, M. and DE LA FUENTE, M. S. 1993. Las tortugas casiquelidias de las calizas litograficas del area Los Catutos, Nequen, Argentina. *Ameghiniana*, **30**, 283–295.

FERNÁNDEZ, M. S. 2007. Redescription and phylogenetic position of *Caypullisaurus* (Ichthyosauria: Ophthalmosauridae). *Journal of Paleontology*, **81**, 368–375.

FISCHER, V. 2012. New data on the ichthyosaur *Platypterygius hercynicus* and its implications for the validity of the genus. *Acta Palaeontologica Polonica*, **57**, 123–134.

FISH, F. E. 1996. Transitions from drag-based to lift-based propulsion in mammalian swimming. *American Zoologist*, **36**, 628–641.

FISH, F. E. 2000. Biomechanics and energetics in aquatic and semiaquatic mammals: platypus to whale. *Physiological and Biochemical Zoology*, **73**, 683–698.

FISH, F. E. 2004. Structure and mechanics of nonpiscine control surfaces. *IEEE Journal of Oceanic Engineering*, **29**, 605–621.

FISH, F. E. and LAUDER, G. V. 2017. Control surfaces of aquatic vertebrates: active and passive design and function. *The Journal of Experimental Biology*, **220**, 4351–4363.

FRAAS, E. 1902. Die meer-crocodilier (Thalattosuchia) des oberen Jura unter specieller berücksichtigung von *Dacosaurus* und *Geosaurus*. *Palaeontographica*, **49**, 1–72.

GEARTY, W., MCCLAIN, C. R. and PAYNE, J. L. 2018. Energetic tradeoffs control the size distribution of aquatic mammals. *Proceedings of the National Academy of Sciences*, **115**, 4194–4199.

GINGERICH, P. D. 2003. Land-to-sea transition in early whales: evolution of Eocene Archaeoceti (Cetacea) in relation to skeletal proportions and locomotion of living semiaquatic mammals. *Paleobiology*, **29**, 429–454.

GOLDBOGEN, J. A. 2018. Physiological constraints on marine mammal body size. *Proceedings of the National Academy of Sciences*, **115**, 3995–3997.

HENDERSON, D. 2006. Floating point: a computational study of buoyancy, equilibrium, and gastroliths in plesiosaurs. *Lethaia*, **39**, 227–244.

HIGHAM, T. E., DAVENPORT, M. S. and JAYNE, B. C. 2001. Maneuvering in an arboreal habitat: the effects of turning angle on the locomotion of three sympatric ecomorphs of *Anolis* lizards. *Journal of Experimental Biology*, **204**, 4141–4155.

HOERNER, S. F. 1965. *Fluid-Dynamic Drag: Practical Information on Aerodynamic Drag and Hydrodynamic Resistance*. Published by S.F. Hoerner, Bakersfield, CA.

HOERNER, S. F. and BORST, H. V. 1985. *Fluid-Dynamic Lift: Practical Information on Aerodynamic and Hydrodynamic Lift*. *In* BORST, H. V. (ed.) Published by L.A. Hoerner, Bakersfield, CA.

JAQUIER, V. P., FRASER, N. C., FURRER, H. and SCHEYER, T. M. 2017. Osteology of a new specimen of *Macrocnemus* aff. *M. fuyuanensis* (Archosauromorpha, Protorosauria) from the Middle Triassic of Europe: potential implications for species recognition and paleogeography of tanystropheid protorosaurs. *Frontiers in Earth Science*, **5**, 1–28.

JI, C., JIANG, D.-Y., RIEPPEL, O., MOTANI, R., TINTORI, A. and SUN, Z.-Y. 2014. A new specimen of *Nothosaurus youngi* from the Middle Triassic of Guizhou, China. *Journal of Vertebrate Paleontology*, **34**, 465–470.

JIANG, D.-Y., MOTANI, R., HAO, W.-C., RIEPPEL, O., SUN, Y.-L., SCHMITZ, L. and SUN, Z.-Y. 2008. First record of Placodontoidea (Reptilia, Sauropterygia, Placodontia) from the Eastern Tethys. *Journal of Vertebrate Paleontology*, **28**, 904–908.

LI, C., JIANG, D.-Y., CHENG, L., WU, X.-C. and RIEPPEL, O. 2013. A new species of *Largocephalosaurus* (Diapsida: Saurosphargidae), with implications for the morphological diversity and phylogeny of the group. *Geological Magazine*, **151**, 100–120.

LIN, K. and RIEPPEL, O. 1998. Functional morphology and ontogeny of *Keichosaurus hui* (Reptilia, Sauropterygia). *Fieldiana Geology New Series*, **39**, 1–35.

LIN, W.-B., JIANG, D.-Y., RIEPPEL, O., MOTANI, R., JI, C., TINTORI, A., SUN, Z.-Y. and ZHOU, M. 2017. A new specimen of *Lariosaurus xingyiensis* (Reptilia, Sauropterygia) from the Ladinian (Middle Triassic) Zhuganpo Member, Falang Formation, Guizhou, China. *Journal of Vertebrate Paleontology*, **37**, e1278703.

LINDGREN, J., JAGT, J. W. M. and CALDWELL, M. W. 2007. A fishy mosasaur: the axial skeleton of *Plotosaurus* (Reptilia, Squamata) reassessed. *Lethaia*, **40**, 153–160.

LINDGREN, J., CALDWELL, M. W. and JAGT, J. W. M. 2008. New data on the postcranial anatomy of the California mosasaur *Plotosaurus bennisoni* (Camp, 1942) (Upper Cretaceous: Maastrichtian), and the taxonomic status of *P. tuckeri* (Camp, 1942). *Journal of Vertebrate Paleontology*, **28**, 1043–1054.

LIU, J. 2013. On the taxonomy of *Xinpusaurus* (Reptilia: Thalattosauria). *Vertebrata PalAsiatica*, **51**, 17–23.

LIU, J., ZHAO, L.-J., LI, C. and HE, T. 2013*a*. Osteology of *Concavispina biseridens* (Reptilia, Thalattosauria) from the Xiaowa Formation (Carnian), Guanling, Guizhou, China. *Journal of Paleontology*, **87**, 341–350.

LIU, J., MOTANI, R., JIANG, D.-Y., HU, S.-X., AITCHISON, J. C., RIEPPEL, O., BENTON, M. J., ZHANG, Q.-Y. and ZHOU, C.-Y. 2013*b*. The first specimen of the Middle Triassic *Phalarodon atavus* (Ichthyosauria: Mixosauridae) from South China, showing postcranial anatomy and peri-Tethyan distribution. *Palaeontology*, **56**, 849–866.

LIVELY, J. R. 2018. Taxonomy and historical inertia: *Clidastes* (Squamata: Mosasauridae) as a case study of problematic paleobiological taxonomy. *Alcheringa: An Australasian Journal of Palaeontology*, **42**, 516–527.

LOMAX, D. R. and MASSARE, J. A. 2017. Two new species of *Ichthyosaurus* from the lowermost Jurassic (Hettangian) of Somerset, England. *Papers in Palaeontology*, **3**, 1–20.

MASSARE, J. A. 1988. Swimming capabilities of Mesozoic marine reptiles: implications for method of predation. *Paleobiology*, **14**, 187–205.

MAYERL, C. J., PRUETT, J. E., SUMMERLIN, M. N., RIVERA, A. R. V. and BLOB, R. W. 2017. Hindlimb muscle function in turtles: is novel skeletal design correlated with novel muscle function? *The Journal of Experimental Biology*, **220**, 2554–2562.

MCGOWAN, C. 1974. A revision of the longipinnate ichthyosaurs of the Lower Jurassic of England, with descriptions of two new species (Reptilia: Ichthyosauria). *Life sciences contributions, Royal Ontario Museum*, **97**, 1–37.

MCGOWAN, C. and MOTANI, R. 2003. Ichthyopterygia. *In* SUES, H.-D. (ed.) *Part 8. Handbook of Paleoherpetology*, Published by F. Pfeil, Munich, Germany, 1–192 pp.

MERRIAM, J. C. 1911. Notes on the relationships of the marine saurian fauna described from the Triassic of Spitzbergen by Wiman. *University of California Publications Bulletin of the Department of Geology*, **6**, 317–332.

MOON, B. C. 2017. A new phylogeny of ichthyosaurs (Reptilia: Diapsida). *Journal of Systematic Palaeontology*, **17**, 129–155.

MOON, B. C. and KIRTON, A. M. 2016. Ichthyosaurs of the British Middle and Upper Jurassic. Part 1, *Ophthalmosaurus*. *Monograph of the Palaeontographical Society*, **170**, 1–84.

MOON, B. C. and KIRTON, A. M. 2018. Ichthyosaurs of the British Middle and Upper Jurassic. Part 2, *Brachypterygius*, *Nannopterygius*, *Macropterygius* and Taxa invalida. *Monographs of the Palaeontographical Society*, **172**, 85–177.

MOTANI, R. 1997. New information on the forefin of *Utatsusaurus hataii* (Ichthyosauria). *Journal of Paleontology*, **71**, 475–479.

MOTANI, R. 1998. Ichthyosaurian relationships illuminated by new primitive skeletons from Japan. *Nature*, **393**, 255–257.

MUELLER-TÖWE, I. J. 2006. Anatomy, phylogeny and palaeoecology of the basal thalattosuchians (Mesoeucrocodylia) from the Liassic of Central Europe. Unpublished PhD thesis, Johannes Gutenberg University Mainz, Mainz, Germanypp.

MUSCUTT, L. E., DYKE, G., WEYMOUTH, G. D., NAISH, D., PALMER, C. and GANAPATHISUBRAMANI, B. 2017. The four-flipper swimming method of plesiosaurs enabled efficient and effective locomotion. *Proceedings of the Royal Society B: Biological Sciences*, **284**, 20170951.

NEENAN, J. M., LI, C., RIEPPEL, O. and SCHEYER, T. M. 2015. The cranial anatomy of Chinese placodonts and the phylogeny of Placodontia (Diapsida: Sauropterygia). *Zoological Journal of the Linnean Society*, **175**, 415–428.

NOSOTTI, S. 2007. *Tanystropheus longobardicus* (Reptilia, Protorosauria): re-interpretations of the anatomy based on new specimens from the Middle Triassic of Besano (Lombardy, northern Italy). *Memorie della Società Italiana di Scienze Naturali e del Museo Civico di Storia Naturale di Milano*, **35**, 1–88.

O'GORMAN, J. P. 2019. Elasmosaurid phylogeny and paleobiogeography, with a reappraisal of *Aphrosaurus furlongi* from the Maastrichtian of the Moreno Formation. *Journal of Vertebrate Paleontology*, **39**, e1692025.

O'KEEFE, F. R. 2002. The evolution of plesiosaur and pliosaur morphotypes in the Plesiosauria (Reptilia: Sauropterygia). *Paleobiology*, **28**, 101–112.

O'KEEFE, F.R. and CARRANO, M. T. 2005. Correlated trends in the evolution of the plesiosaur locomotor system. *Paleobiology*, **31**, 656–675.

OLSEN, P. E. 1979. A new aquatic eosuchian from the Newark Supergroup (Late Triassic–Early Jurassic) of North Carolina and Virginia. *Postilla*, **176**, 1–14.

PÁRAMO-FONSECA, M. E. 2014. *Eonatator coellensis* nov. sp. (Squamata: Mosasauridae), nueva especie del cretácico superior de Colombia. *Revista de la Academia Colombiana de Ciencias Exactas, Físicas y Naturales*, **37**, 499.

PÉREZ-GARCÍA, A., DE LA FUENTE, M. S. and ORTEGA, F. 2012. A new freshwater basal eucryptodiran turtle from the Early Cretaceous of Spain. *Acta Palaeontologica Polonica*, **57**, 285–298.

RABI, M., ZHOU, C.-F., WINGS, O., GE, S. and JOYCE, W. G. 2013. A new xinjiangchelyid turtle from the Middle Jurassic of Xinjiang, China and the evolution of the basipterygoid process in Mesozoic turtles. *BMC Evolutionary Biology*, **13**, 1–29.

REIDENBERG, J. S. 2007. Anatomical adaptations of aquatic mammals. *The Anatomical Record: Advances in Integrative Anatomy and Evolutionary Biology*, **290**, 507–513.

RENESTO, S. and TINTORI, A. 1995. Functional morphology and mode of life of the late Triassic placodont *Psephoderma alpinum* Meyer from the Calcare di Zorzino (Lombardy, Italy). *Rivista Italiana di Paleontologia e Stratigrafia*, **101**, 37–48.

RIEPPEL, O. 2000. *Paraplacodus* and the phylogeny of the Placodontia (Reptilia: Sauropterygia). *Zoological Journal of the Linnean Society*, **130**, 635–659.

RIEPPEL, O., JINLING, L. and JUN, L. 2003. *Lariosaurus xingyiensis* (Reptilia: Sauropterygia) from the Triassic of China. *Canadian Journal of Earth Sciences*, **40**, 621–634.

RIEPPEL, O., LI, C. and FRASER, N. C. 2008. The skeletal anatomy of the triassic protorosaur *Dinocephalosaurus orientalis* Li, from the Middle Triassic of Guizhou Province, southern China. *Journal of Vertebrate Paleontology*, **28**, 95–110.

RIVERA, A. R. V. and W. BLOB, R. 2010. Forelimb kinematics and motor patterns of the slider turtle (Trachemys scripta) during swimming and walking: shared and novel strategies for meeting locomotor demands of water and land. *Journal of Experimental Biology*, **213**, 3515–3526.

RIVERA, A. R., RIVERA, G. and BLOB, R. W. 2013. Forelimb kinematics during swimming in the pig-nosed turtle, *Carettochelys insculpta*, compared with other turtle taxa: rowing versus flapping, convergence versus intermediacy. *Journal of Experimental Biology*, **216**, 668–680.

RUSSELL, D. A. 1967. Systematics and morphology of American mosasaurs. *Bulletin of the Peabody Museum of Natural History*, **23**, 1–254.

SACHS, S. and KEAR, B. P. 2017. Redescription of the elasmosaurid plesiosaurian *Libonectes atlasense* from the Upper Cretaceous of Morocco. *Cretaceous Research*, **74**, 205–222.

SANDER, P. M. 1989. The pachypleurosaurids (Reptilia: Nothosauria) from the Middle Triassic of Monte San Giorgio (Switzerland) with the description of a new species. *Philosophical Transactions of the Royal Society London B*, **325**, 561–666.

SCHEYER, T. M., NEENAN, J. M., BODOGAN, T., FURRER, H., OBRIST, C. and PLAMONDON, M. 2017. A new, exceptionally preserved juvenile specimen of

Eusaurosphargis dalsassoi (Diapsida) and implications for Mesozoic marine diapsid phylogeny. *Scientific Reports*, **7**, 1–22.

SCHINDELIN, J., ARGANDA-CARRERAS, I., FRISE, E., KAYNIG, V., LONGAIR, M., PIETZSCH, T., PREIBISCH, S., RUEDEN, C., SAALFELD, S., SCHMID, B., TINEVEZ, J.-Y., WHITE, D. J., HARTENSTEIN, V., ELICEIRI, K., TOMANCAK, P. and CARDONA, A. 2012. Fiji: an open-source platform for biological-image analysis. *Nature Methods*, **9**, 676–682.

SCHMITZ, L., SANDER, P. M., STORRS, G. W. and RIEPPEL, O. 2004. New Mixosauridae (Ichthyosauria) from the Middle Triassic of the Augusta Mountains (Nevada, USA) and their implications for mixosaur taxonomy. *Palaeontographica Abteilung A*, **270**, 133–162.

SHAO, S., LI, L., YANG, Y. and ZHOU, C.-F. 2018. Hyperphalangy in a new sinemydid turtle from the Early Cretaceous Jehol Biota. *PeerJ*, **6**, e5371.

SHIKAMA, T., KAMEI, T. and MURATA, M. 1978. Early Triassic Ichthyosaurus *Utatsusaurus hataii* Gen. et sp. nov. from the Kitakami Massif, Northeast Japan. *Tohoku University Scientific Report*, **48**, 77–97.

SMITH, A. S. 2007. Anatomy and systematics of the rhomaleosauridae (Sauropterygia: Plesiosauria). Unpublished PhD thesis, National University of Ireland, Dublin, Ireland, 301pp.

SMITH, A. S. 2015. Reassessment of *'Plesiosaurus' megacephalus* (Sauropterygia: Plesiosauria) from the Triassic-Jurassic boundary, UK. *Palaeontologia Electronica*, **18**, 1–20.

SOUL, L. C. and BENSON, R. B. J. 2017. Developmental mechanisms of macroevolutionary change in the tetrapod axis: A case study of Sauropterygia. *Evolution*, **71**, 1164–1177.

STERNBERG, C. H. (Charles H. 1909. *The Life of a Fossil Hunter*. Published by H. Holt, New York.

TONG, H. and BRINKMAN, D. 2013. A new species of *Sinemys* (Testudines: Cryptodira: Sinemydidae) from the Early Cretaceous of Inner Mongolia, China. *Palaeobiodiversity and Palaeoenvironments*, **93**, 355–366.

TONG, H., JI, S.-A. and JI, Q. 2004. *Ordosemys* (Testudines: Cryptodira) from the Yixian Formation of Liaoning Province, Northeastern China: New Specimens and Systematic Revision. *American Museum Novitates*, **3438**, 1–20.

TONG, H., HIRAYAMA, R. and MAKHOUL, E. 2006. *Rhinochelys* (Chelonioidea: Protostegidae) from the Late Cretaceous (Cenomanian) of Nammoura, Lebanon. *Atti della Società italiana di scienze naturali e del Museo civico di storia naturale di Milano*, **147**, 113–138.

VINCENT, P. 2011. Re-examination of *Hauffiosaurus zanoni*, a pliosauroid from the Toarcian (Early Jurassic) of Germany. *Journal of Vertebrate Paleontology*, **31**, 340–351.

WANG, W., LI, C. and WU, X.-C. 2018. An adult specimen of *Sinocyamodus xinpuensis* (Sauropterygia: Placodontia) from Guanling, Guizhou, China. *Zoological Journal of the Linnean Society*, **185**, 910–924.

WANG, W., MA, F. and LI, C. 2019. First subadult specimen of *Psephochelys polyosteoderma* (Sauropterygia, Placodontia) implies turtle-like fusion pattern of the carapace. *Papers in Palaeontology*, **6**, 251–264.

WEBER, P. W., HOWLE, L. E., MURRAY, M. M. and FISH, F. E. 2009. Lift and drag performance of odontocete cetacean flippers. *Journal of Experimental Biology*, **212**, 2149–2158.

WEBER, P. W., HOWLE, L. E., MURRAY, M. M., REIDENBERG, J. S. and FISH, F. E. 2014. Hydrodynamic performance of the flippers of large-bodied cetaceans in relation to locomotor ecology. *Marine Mammal Science*, **30**, 413–432.

WELLES, S. P. 1943. Elasmosaurid plesiosaurs with description of new material from California and Colorado. *Memoirs of the University of California*, **13**, 125–254.

WELLES, S. P. 1962. A new species of elasmosaur from the Aptian of Colombia and a review of the Cretaceous plesiosaurs. *University of California Publications in Geological Sciences*, **44**, 1–96.

WELLES, S. P. and BUMP, J. D. 1949. *Alzadasaurus pembertoni* , a New Elasmosaur from the Upper Cretaceous of South Dakota. *Journal of Paleontology*, **23**, 521–535.

WILD, R. 1980. Neue funde von *Tanystropheus*. *Schweizerische Paläontologische Abhandlungen*, **102**, 1–44.

WU, X.-C., ZHAO, L.-J., SATO, T., GU, S.-X. and JIN, X.-S. 2016. A new specimen of *Hupehsuchus nanchangensis* Young, 1972 (Diapsida, Hupehsuchia) from the Triassic of Hubei, China. *Historical Biology*, **28**, 43–52.

XIAOFENG, W., BACHMANN, G. H., HAGDORN, H., SANDER, P. M., CUNY, G., XIAOHONG, C., CHUANSHANG, W., LIDE, C., LONG, C., FANSONG, M. and GUANGHONG, X. 2008. The Late Triassic black shales of the Guanling area, Guizhou province, South-West China: a unique marine reptile and pelagic crinoid fossil lagërstatte. *Palaeontology*, **51**, 27–61.

YOUNG, J. W., DANCZAK, R., RUSSO, G. A. and FELLMANN, C. D. 2014. Limb bone morphology, bone strength, and cursoriality in lagomorphs. *Journal of Anatomy*, **225**, 403–418.

ZAMMIT, M., DANIELS, C. B. and KEAR, B. P. 2008. Elasmosaur (Reptilia: Sauropterygia) neck flexibility: Implications for feeding strategies. *Comparative Biochemistry and Physiology Part A: Molecular & Integrative Physiology*, **150**, 124–130.

ZHOU, C.-F. 2010. A new eucryptodiran turtle from the Early Cretaceous Jiufotang Formation of western Liaoning, China. *Zootaxa*, **2676**, 45–56.

ZHOU, C.-F. and RABI, M. 2015. A sinemydid turtle from the Jehol Biota provides insights into the basal divergence of crown turtles. *Scientific Reports*, **5**, 16299.